DESIGN OPTIMIZATION AND TESTING OF COMBINED CENTRIFUGAL SEPARATION AND COMPRESSION TECHNOLOGY

by
William Maier
Principal Engineer
and
Yuri Biba
Senior Aero Performance Engineer
Dresser-Rand Company
Olean, New York

William Maier is a Principal Engineer with Dresser-Rand Company, in Olean, New York. His latest activities are centered on the integration of separation technologies with high-speed turbomachinery.

Mr. Maier received a B.Sc. degree (Mechanical Engineering, 1981) from Rochester Institute of Technology.

Yuri Biba is a Staff Aero Performance Engineer with Dresser-Rand Company, in Olean, New York. He has been involved in aerodynamic design and analysis, performance prediction, and optimization of centrifugal compressor components.

Mr. Biba received his M.Sc. degree (Aeronautical Engineering, 1984) and Ph.D. degree (Mechanical Engineering, 1987) from St.Petersburg State Polytechnic University, Russia. He has authored technical papers on the subject of turbomachinery aerodynamics and is a member of ASME.

ABSTRACT

The relatively new technology of rotary gas-liquid separation has been advanced by the development of a rotating centrifugal separator closely coupled to a centrifugal turbocompressor. This development by a major equipment manufacturer included the creation and calibration of an integrated design suite, and the use of this tool to optimize a separator/compressor stage. The compression and separation performance of this design was verified by building test hardware and testing it in the original equipment manufacturer's (OEM's) multiphase flow loop. Overall test results agreed well with performance predicted by the design tools.

INTRODUCTION

Conventional technology for separation of liquids from gases is well developed in the petroleum industry. Reliable separation technologies based on gravity settling have been available for many years. The simplest form of separation is embodied in a horizontal bulk separation tank as shown in Figure 1. The economics of oil and gas production, deriving from fields with smaller recoverable reserves and/or deepwater environments, are continuously driving the need for further improvement over current methods to reduce the cost of development and operation.

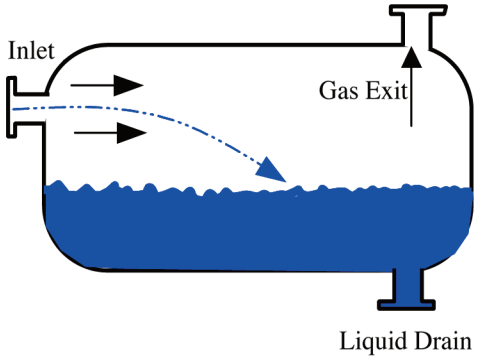

Figure 1. Classic Bulk Tank Separation.

Recently, gains in separator size reduction and effectiveness have been realized through the use of complex internals for separator vessels including inlet devices, swirl tubes, and demisting pads. Representative diagrams of these types of separation enhancement are shown in Figure 2.

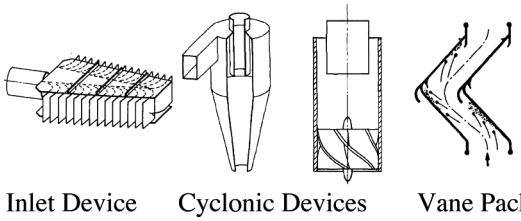

Figure 2. Advanced Static Separation Devices after Swanborn (1988).

Even with these improvements, advanced static separators are still burdened with relatively large footprint and weight characteristics that require substantial support structures when used offshore and are still expensive to transport and install.

The authors' company has been active in developing a promising new separation technology based on rotating centrifugal separation principles. Static separation has inherent limits on through-flow velocities due to the combination of flooding and liquid reentrainment effects. These velocity limits directly translate into ultimate lower limits on the physical size and weight of such devices. Because of its utilization of rotating separation surfaces, rotating centrifugal separation technology overcomes these limitations and potentially allows for a step change in separator size. Foundation work on rotating separation was done with standalone devices as described in Rawlins and Ross (2000), Rawlins and Ross (2001), and Ross, et al. (2001). More recently, work has focused on developing a rotating centrifugal separator as an inlet stage for multistage centrifugal turbocompressors (Chochua, et al., 2008).

This paper details the process implemented for development of this new separator technology from tool development and design optimization through prototype testing in a multiphase flow loop.

ROTARY SEPARATION

By far the most common means of separating gas and liquids in the oil and gas industry is through density-based separation. Centrifugal rotating separation is also of this type. In many ways rotating centrifugal separation is similar to static cyclonic separation; swirl is induced in the mixed fluid stream resulting in an augmentation of body forces. Higher density liquids are forced to larger radii and the lower density gas tends toward smaller radii. The difference between the two technologies is the amount of separation force augmentation possible. The simplest bulk tank devices use earth's gravity or 1G of acceleration to separate fluids by density. Most single-body static cyclones use less than 100Gs (Oxley, et al., 2003), but some special multicyclone scrubbers can attain accelerations in excess of 2,000Gs (Austrheim, 2006). Going to very high augmentation in a static configuration can actually result in diminished separation because increased shear forces near the outer wall start to lift liquid off the surface and reentrain it into the main gas stream. In the centrifugal rotating separator, this shear force is greatly reduced because the wall is traveling at a velocity similar to the gas. Additionally, because of the outer wall's rotation, liquid adhered to the wall "feels" a body force that continues to force it against the wall. With this freedom of design, accelerations as high as 7,000Gs have been utilized successfully in rotary separators. Figure 3 is a cross section of a rotary separator and Figure 4 is a labeled schematic representation of the separator. Major components include a swirl generator, a rotating drum, and a liquid collector.

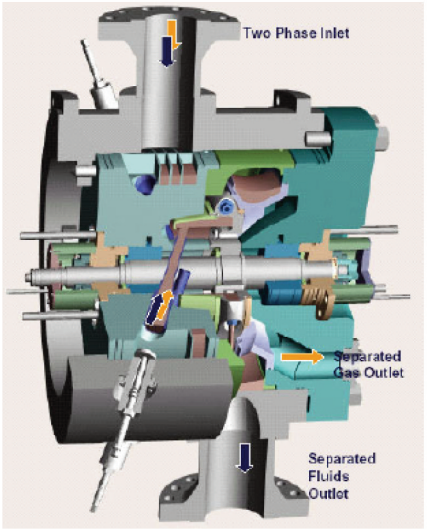

Figure 3. 32,000 BPD Biphase RST after Oxley et al. (2003).

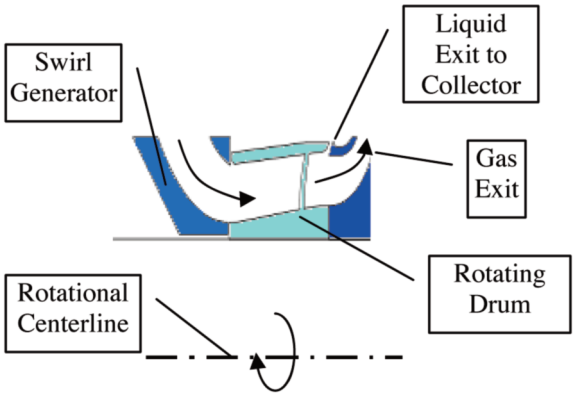

Figure 4. Rotary Separator Cross Section.

The following is a review of the physics of the rotary separation process leading to the derivation of a global separation parameter. This nondimensional parameter can be used to compare the performance of rotating centrifugal separators of differing physical shape, operating with various process conditions. This derivation follows from a similar treatment of static cyclonic separators (Hoffmann and Stein, 2002). Consider the liquid droplet in a rotary separator shown schematically in Figure 5. For this analysis it is assumed that the multiphase stream is flowing from left to right at velocity (V_{axial}) and the separator drum is rotating about the axis shown at pitch-line rotational velocity U. Droplets are assumed to maintain a spherical shape and uniform size.

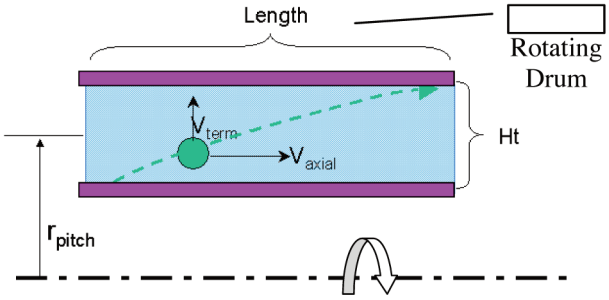

Figure 5. Rotating Centrifugal Separator Schematic.

The fluid rotation induces a centrifugal body force on the droplet that results in acceleration to a terminal radial migration velocity (V_{term}) for the droplet with respect to the gas stream. The efficiency of liquid separation is approximately proportional to the ratio of terminal to axial velocity and the ratio of axial length to radial height of the physical separator flowpath. Large terminal velocity and axial length result in higher efficiency whereas relatively large axial velocity and radial height reduce separation performance. This is expressed mathematically in Equation (1).

$$\eta_{sep} \propto \left[V_{term} / V_{Axial} \right] \times \left[Length / Ht \right] \tag{1}$$

The terminal velocity is a difficult value to determine, especially for liquid particles. To estimate V_{term}, a summation of several opposing forces imposed on the droplet has to be made. This is shown in the free body diagram of the liquid droplet in Figure 6, and expressed in Equation (2).

$$\sum \bar{F}_{rad} = m_{drop} \bar{a}_{drop} = 0 \tag{2}$$

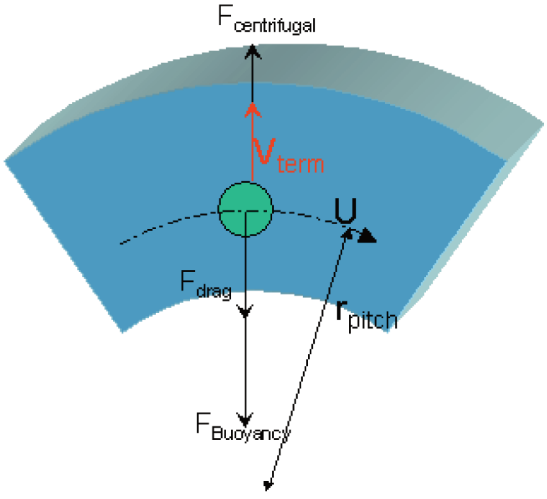

Figure 6. Droplet Free Body Diagram of Droplet.

The sum of these forces initially acts to accelerate the droplets in the outer radial direction until equilibrium between the inertial forces and the drag force is reached. At this point, the acceleration of the droplets goes to zero and their radial velocity becomes a constant terminal velocity. The following three equations define the magnitude of the forces on the droplets in terms of droplet diameter.

$$\left|\overline{F}_{cent}\right| = \left(\pi D_{drop}^{3} \Big/ 6\right) \rho_{liq} a_{sep} \tag{3}$$

$$\left|\overline{F}_{bouyancy}\right| = \left(\pi D_{drop}^{3} \Big/ 6\right) \rho_{gas} a_{sep} \tag{4}$$

$$\left|\overline{F}_{Drag}\right| = \frac{1}{2} Cd \left(\pi D_{drop}^{2} \Big/ 4\right) \rho_{gas} V_{term}^{2} \tag{5}$$

Where the centrifugal acceleration on the droplet is defined in Equation (6):

$$a_{sep} = U^{2} \Big/ r_{drum} \tag{6}$$

The drag coefficient in Equation (5) is a function of droplet Reynolds number. The following is an approximate correlation for spherical droplet drag (White, 1974).

$$Cd = \frac{24}{\mathrm{Re}} + \frac{6}{1+\sqrt{\mathrm{Re}}} + .40 \tag{7}$$

Equation (8) is a rearrangement of Equations (2) through (7) solving for terminal velocity in terms of droplet diameter and drag coefficient.

$$V_{term} = \sqrt{\left(\frac{4}{3}\frac{a_{sep}}{C_d}\right) D_{drop} \frac{(\rho_{liq} - \rho_{gas})}{\rho_{gas}}} \tag{8}$$

Equation (8) is similar to the Souders-Brown equation commonly used to characterize static separators (Souders and Brown, 1934). The difference here is that the acceleration term and the drag coefficient are referred to conditions in a turbomachine rotational reference frame rather than the acceleration of gravity and the Stokes drag regime normally encountered in static separators.

A problematic variable in the above analysis is liquid droplet size. Unfortunately, with gas-liquid separation, the liquid droplet size distribution varies both spatially and temporally and is not easily determined analytically. A modification of a semiempirical correlation is used here to estimate a characteristic liquid droplet size (Azzopardi, et al., 1980). This correlation, Equation (9), is based on a gas Reynolds number and a Weber number referenced to global properties and flow conditions of the gas stream.

$$D_{drop} = f\left(d_{Hyd}, Re, We, \left(\frac{\rho_{gas}}{\rho_{liq}}\right)\right) \tag{9}$$

Equations (1), (8), and (9) can be combined to define a separation parameter that is an alternate expression for the ratio of separation velocity to through-flow velocity as expressed in Equations (10) and (11).

$$\eta_{sep} \propto \left[\frac{1}{SP}\right] \times \left[Length \Big/ Ht\right] \tag{10}$$

$$SP = \frac{V_{Axial}}{\sqrt{\left(\frac{4}{3}\frac{a_{sep}}{Cd}\right) D_{drop} \frac{(\rho_{liq} - \rho_{gas})}{\rho_{gas}}}} \tag{11}$$

The resulting separation parameter (SP) is a nondimensional number that gives an indication of the degree of difficulty of rotating centrifugal separation for a given set of basic separator geometry and process conditions. All geometry is referred to the separator drum inlet. Separator length and passage height terms are left out of the expression for separation parameter as they are considered independent design parameters. The formulation of the parameter is such that a larger value denotes more difficult separation conditions.

DESIGN PROCESS

Due to inherently tight coupling of the centrifugal rotating separator flowpath and the downstream centrifugal compressor, a novel and comprehensive design methodology was followed to help assure a high level of optimization. The process is shown schematically in Figure 7.

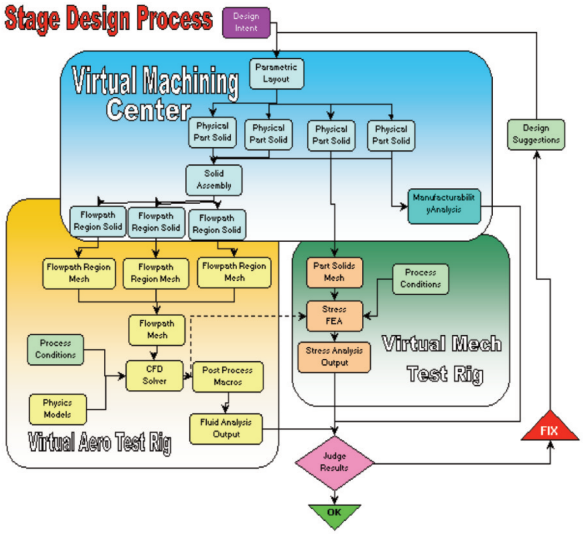

Figure 7. Separator Stage Optimization Process.

The basis for the design methodology adopted here is a parametric rules-based solid model. With this system, a master layout composed of a series of interlinked parametric 2-D curves completely define the topology of the separator/compressor stage. These 2-D curves simultaneously define individual part solids, spatial relationships between parts, and fluid volumes used in computational fluid dynamics (CFD) analysis. This master layout is referenced by all component part models and flowpath domain models. In a sense, the master layout acts like a genetic code for the separator, where it provides specific information about a component's own geometry, as well as information about the complete separator assembly. The relationship between physical parts and the parametric master layout is shown in Figure 8.

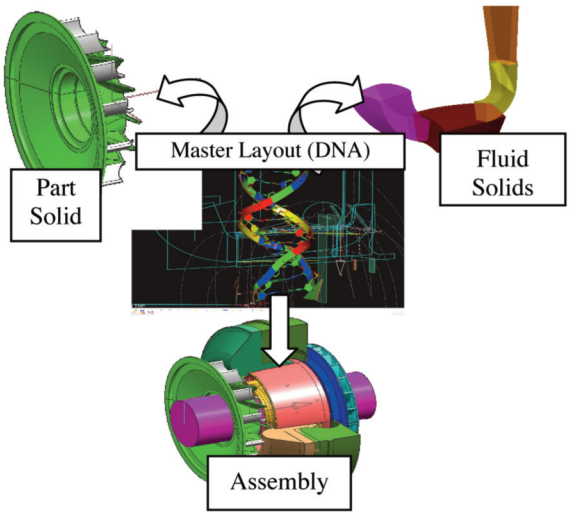

Figure 8. Genetic Master Geometry Layout.

CFD meshing and analysis are then performed on the newly generated geometry. This CFD analysis method was developed around a commercially available CFD code. To maximize connectivity, the

fluid domain created in the geometry generation phase is divided into multiple regions with a consistent naming convention for both regions and faces. These fluid domains can span across multiple physical part solids. Modeling multiphase fluid is a challenging task, especially with the conditions typically encountered in a rotating centrifugal separator. After significant development, the model chosen included an Eulerian-Eulerian formulation with a k-epsilon turbulence model. It utilized an inhomogeneous multiple size group model (MUSIG) (Kreppera, et al., 2008) with droplet breakup.

The CFD model was tuned by comparing its results with several test cases for which actual test results were available. The first test case was a set of two existing empirical bulk flow liquid particle size models including the Harwell model and a method based on Hinze (Mondt, 2005) for steady state pipe flow. For the CFD calibration, a multiphase stream was introduced into a very long constant diameter pipe. The resulting average liquid particle size (D32) at the exit of the pipe was noted. This was repeated for different bulk gas velocities in the pipe. The results of these CFD calculations were compared to the Harwell and Hinze models for the same pipe flow conditions in Figure 9 where terminal droplet size is plotted for various bulk gas velocities. There is generally good agreement between the models, but the CFD solution tends to over-predict the particle size at higher velocities. This figure also gives an idea of the representative droplet sizes experienced in a typical rotating centrifugal separator operating at high pressure with hydrocarbon fluids.

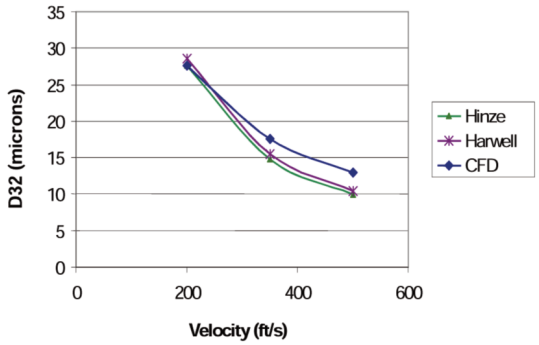

Figure 9. CFD Comparison with Empirical Droplet Size Correlations.

Figure 10 is a representative output from the calibrated CFD modeling tool for an intermediate optimization solution of a rotating centrifugal separator.

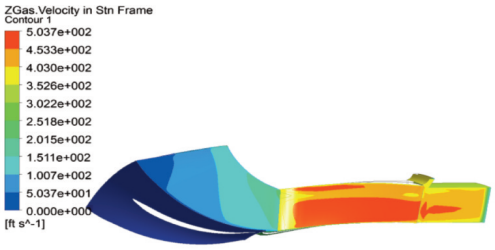

Figure 10. CFD Prediction of Gas Velocity Field.

Separation efficiency, aerodynamic compression performance, and axial length were considered in a multiobjective optimization. Because of the complex nature of the coupling between these output variables and separator geometry, a simple manual method using features of the random walk and hill-climbing techniques (Winston, 1992) combined with expert knowledge was used. The random walk method is where the multidimensional design space is explored in various random directions around a starting point in order to understand the local topology (e.g., hills, valleys, and cliffs in a 3-D domain). The hill climbing method is where local gradients in the objective function are studied and succeeding iterations are targeted at directions that give increased slope (for maximizing the objective function). Both of these methods are graphically depicted for a 3-D solution domain in Figure 11. Figure 12 displays the progression of the optimization process through 16 major iterations. The final design iteration suggested a 15 percent improvement in separation performance and a 17 percent improvement in compression efficiency relative to the initial baseline design.

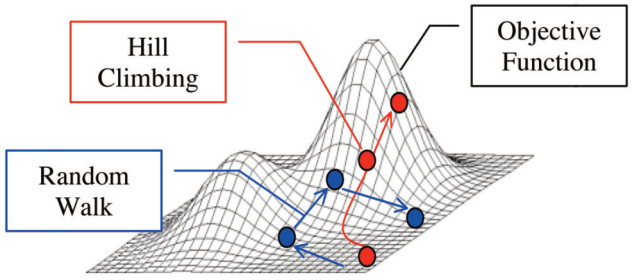

Figure 11. Optimization Methods Used.

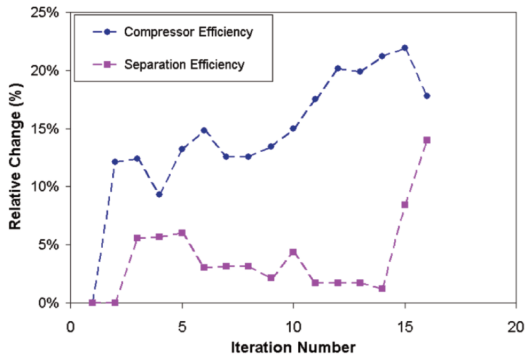

Figure 12. Separator Stage Optimization Progression.

PHYSICAL MULTIPHASE TESTING

After analytical optimization was performed, a shop test was carried out on the optimized solution at the OEM's multiphase test facility in Olean, New York. The test facility is based on a relatively standard compressor test loop. Run in parallel with the gas portion of the loop is a complete liquid supply and monitoring system. Additional equipment in the liquid portion includes a supply/receiver tank, a delivery pump, an injection port, flow meters, and a secondary separator. The liquid injection port utilized an array of misting nozzles and was designed to provide fully dispersed atomized liquid flow. A schematic of the multiphase loop is given in Figure 13. A rendering of the injection port is shown in Figure 14. A photograph of the test loop and rig are shown in Figures 15 and 16.

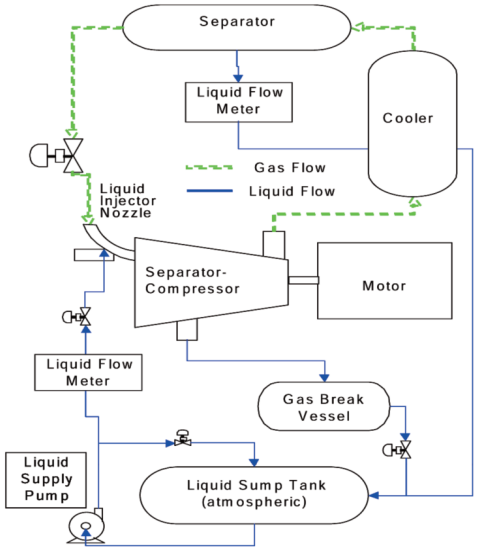

Figure 13. Multiphase Flow Loop Schematic.

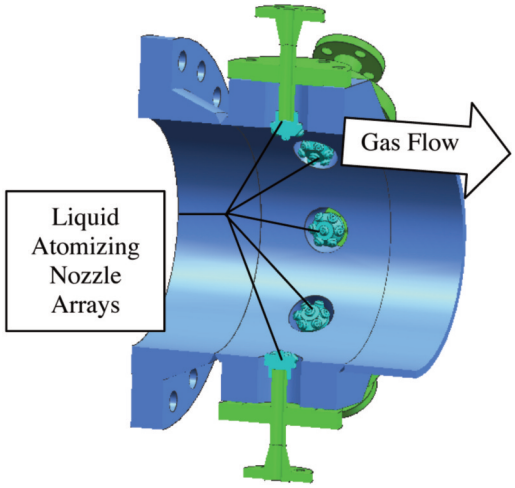

Figure 14. Liquid Injection Nozzle.

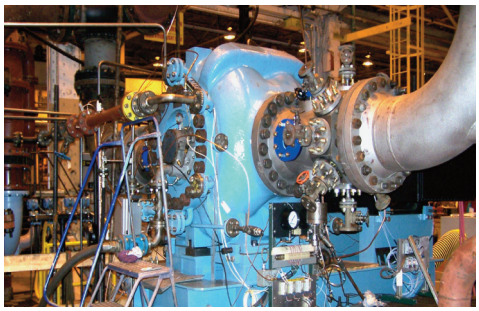

Figure 15. Multiphase Flow Loop Photograph.

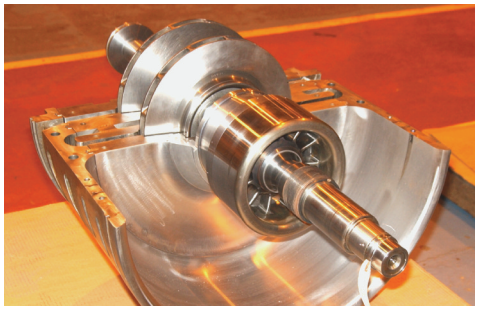

Figure 16. Test Hardware.

Test instrumentation included total pressure and total temperature probes in order to obtain as-tested compressor performance information by collecting data upstream and downstream of the separator stage.

Separation efficiency was measured with a mass balance on the liquid stream, comparing the amount of liquid introduced into the loop to the amount of liquid carryover collected by the downstream secondary separator as defined in Equation (12).

$$\eta_{sep} = \left(\dot{m}_{in} - \dot{m}_{co}\right) \Big/ \dot{m}_{in} \qquad (12)$$

Where:

η_{sep} - Separation efficiency

$\dot{m}_{in}$ - Input liquid mass flowrate

$\dot{m}_{co}$ - Carryover liquid mass flowrate

Table 1 summarizes the range of test conditions. All testing was done with nitrogen gas. The liquid used for separation testing was the hydrocarbon solvent D-60, commonly used for simulating condensate in gas-liquid separation testing.

Table 1. Test Condition Summary.

Parameter	Units	Min.	Max
Suction Pressure	Psia (Pa)	40 (276,000)	300 (2,068,000)
Gas Flow	ACFM (m^3/min)	1500 (32.6)	3100 (94.4)
Liquid Flow (LGMR)	-	0.05	1.0
Rotational Speed	rpm (Hz)	9,000 (150)	13,500 (225)

TEST RESULTS

Over 200 dry test points and 300 wet points were recorded during testing.

Figure 17 is a plot of separation efficiency versus the separation parameter as derived above, and liquid loading for all of the multiphase test data.

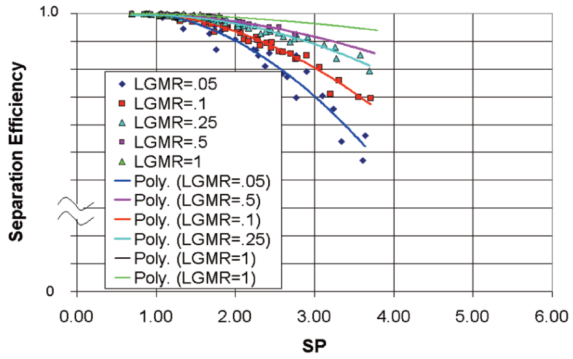

Figure 17. Experimental Separation Performance as a Function of SP and Liquid Loading.

The liquid loading is expressed here as the ratio of liquid to gas mass flowrates (LMGR). The test data suggest a consistent trend of lower separation efficiency with both increasing SP and decreasing LMGR. Figure 18 compares test data with the complex multiphase CFD predictions. For this comparison different rotational speeds and gas flows were run with liquid flow and liquid and gas properties held constant.

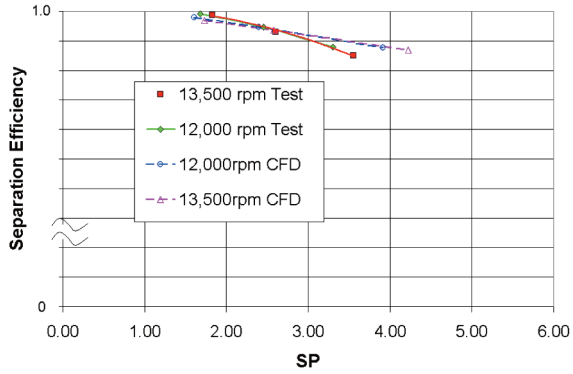

Figure 18. Test Versus CFD Prediction.

It is clear from the figure that SP takes rotational speed into account as both test and complex multiphase CFD speed data lay on the same line. The complex multiphase CFD prediction, while agreeing closely with test data at the design point, has a different slope with respect to gas flow. The test data show a more severe negative effect on separation efficiency with increasing gas flowrates than that predicted with the complex multiphase CFD model.

It is insightful to compare the experimental separation test results obtained here with current state-of-the-art static separation methodologies. This is shown in Figure 19, which compares experimentally measured separation performance and representative through velocities of various static separation technologies (Austrhiem, 2006) with a rotating centrifugal separator at similar fluid conditions. There is a tenfold increase in operational velocities for advanced rotary separation over static technologies. This characteristic velocity correlates strongly with separator size and weight.

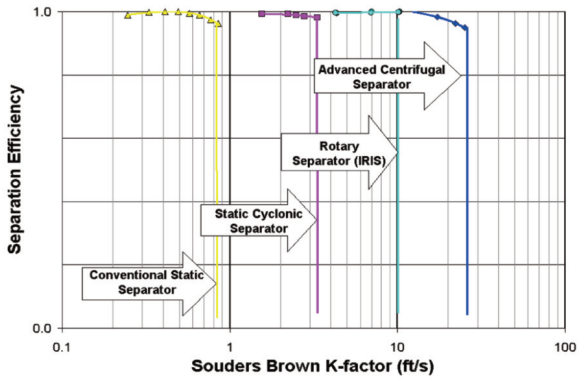

Figure 19. Comparison of Separation Technologies.

To assess compression performance of the rotating centrifugal separator stage, a series of dry gas test runs was executed. The rotating centrifugal separator imparts a substantial circumferential component to gas velocity exiting the separator drum and entering the first stage of compression. If the first stage was the OEM's standard configuration, selected for the target speed and flow rate, a deswirling arrangement would be required to mitigate the effect of this prewhirl. An alternative solution, which was finally chosen, utilized a modification to the downstream impeller design to accept flow conditions at the separator drum exit. Simultaneously, this new impeller design, along with design of downstream stationary components, ensured preserving head level and gas volume reduction relative to the OEM's standard compression stage.

For compressor performance, the rotating centrifugal separator is considered an integral part of the first stage, which may be called a separator/compressor stage. This combination allows calculating the overall compressor performance using the OEM's standard practices and configuring a separator/compressor system for target conditions in the same way as conventional compressor units are typically configured.

Based on results of the CFD model, an array of performance correction factors was generated. Predicted performance curves for this prototype separator/compressor stages were then calculated by applying these corrections to a simplified mean-line compressor performance model. It turns out that the actual total pressure losses in the separator flowpath are similar to typical turbomachine primary flow passage losses. As shown in Figure 20, initial mean-line performance estimates correlate well with test data for a wide range of flow rates and rotational speeds. The test results clearly validate this methodology for separator/compressor stage performance prediction, suggesting an accurate production prediction tool can be developed based on this modeling concept.

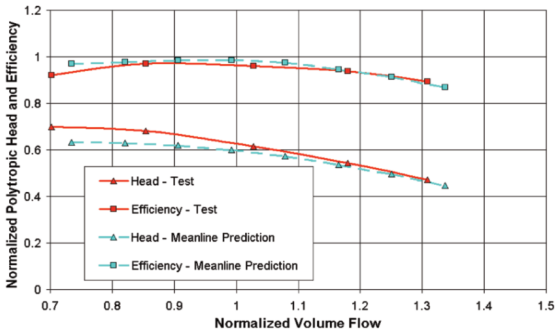

Figure 20. Separator/Compressor Stage Performance Comparison with Mean-line Prediction.

CONCLUSIONS

The OEM has developed a novel rotating centrifugal density-based separation technology. The development included the creation of a virtual reality stage design suite with a calibrated complex multiphase CFD modeling tool and mean-line performance extensions. This design suite was used to optimize the design of the separator in terms of compressor and separator performance. Testing of prototype hardware was then carried out in a multiphase flow loop. The results of testing confirm the suitability of the predicting models.

This design and experimental testing exercise confirm the promise of rotary separation technology to push separation into a new regime of compactness compared to current state-of-the-art static separation methodologies. The potential for a step change in separator size with comparable performance is therefore realized with this novel technology.

NOMENCLATURE

Latin Letters

a	= Acceleration
C_d	= Drag coefficient
D	= Diameter
D32	= Sauter mean diameter
F	= Force
Ht	= Drum passage height
Length	= Drum axial length
LGMR	= Liquid to gas mass flow ratio
m	= Mass
r	= Radius
R^2	= Square of correlation coefficient
Re	= Reynolds number
SP	= Separation parameter
SP'	= Separation parameter normalized to GLMR=0.1
U	= Pitch-line wheel speed
V	= Velocity
We	= Weber number

Greek Letters

η	= Efficiency
μ	= Absolute viscosity
ρ	= Density
σ	= Interfacial surface tension

Subscripts

axial	= Axial component
drop	= Droplet
drum	= Separator drum
gas	= Gas
Hyd	= Hydraulic
liq	= Liquid
pitch	= Pitch line
radial	= Radial component
sep	= Separator
term	= Terminal

REFERENCES

Austrheim, T., 2006, "Experimental Characterization of High-Pressure Natural Gas Scrubbers," Ph.D. Thesis, University of Bergen, pp. 122-124.

Azzopardi, B. J., Freeman, G., and King, D. J., 1980, "Drop Sizes and Deposition in Annular Two-Phase Flow," UKAEA Report AERE-R9634.

Chochua, G., Gilarranz, J., Kidd, H. A., and Maier, W., 2008, "A DNV Modeled Qualification Process for a Turbocompressor Incorporating a Rotary Separator Known as the Integrated Compression System," *Proceedings of the Thirty-Seventh Turbomachinery Symposium*, Turbomachinery Laboratory, Texas A&M University, College Station, Texas, pp. 111-118.

Hoffmann, A. C. and Stein, L. E., 2002, *Gas Cyclones and Swirl Tubes*, Berlin, Germany: Springer-Verlag, pp. 19-23.

Kreppera, E., Lucasa, D., Frankb, T., Prasserc, H., and Zwart, P., July 2008, "The Inhomogeneous MUSIG Model for the Simulation of Polydispersed Flows," *Nuclear Engineering and Design*, *238*, (7), pp. 1690-1702.

Maier, W., Chochua, G., and Biba, Y., 2010, "Development of a Rotating Centrifugal Separator Technology for Centrifugal Compressors," GT2010-22222, Proceedings of ASME Turbo Expo 2010, Glasgow, United Kingdom.

Mondt, E., 2005, "Compact Centrifugal Separator of Dispersed Phases," Ph.D. Thesis, Eindhoven University Press, pp. 61-63.

Oxley, K. C., Bennett, J. R., Fremin, L. O., Taylor, J. D., and Ross, G. D., 2003, "RST's Mission to Mars—The First Commercial Application of Rotary Separator Turbine Technology," Paper 15357, Presented at the Offshore Technology Conference, Houston, Texas.

Rawlins, C. H. and Ross, G. D., 2000, "Design and Analysis of a Multiphase Turbine for Compact Gas-Liquid Separation," Paper 63039, Presented at the 2000 SPE Annual Technology Conference and Exhibition, Dallas, Texas.

Rawlins, C. H. and Ross, G. D., 2001, "Field Results of a Rotary Separator Turbine on the Ram/Powell TLP," Paper 13218, Presented at the 2001 Offshore Technology Conference, Houston, Texas.

Ross, G. D., Oxley, K. C., and Rawlins, C. H., 2001, "Analysis of Results of a Rotary Separator Turbine on the Shell Ram-Powell TLP," Presented at the BHR Group Limited's 10th International Conference Multiphase '01, Cannes, France.

Souders, M. and Brown, G. G., 1934, "Design of Fractionating Columns. I. Entrainment and Capacity," *Industrial & Engineering Chemistry*, *26*, pp. 98-103.

Swanborn, R. A., 1988, "A New Approach to the Design of Gas-Liquid Separators for the Oil Industry, Ph.D. Thesis, Technical University Delft, Netherlands.

White, F. M., 1974, *Viscous Fluid Flow*, New York, New York: McGraw-Hill, pp. 204-210.

Winston, P. H., 1992, *Artificial Intelligence*, Third Edition, Reading, Massachusetts: Addison-Wesley Publishing Company, pp. 70-72.